Journal of Hazardous Materials 347 (2018) 252–265

Contents lists available at ScienceDirect

Journal of Hazardous Materials

journal homepage: www.elsevier.com/locate/jhazmat

Selective formation of copper nanoparticles from acid mine drainage using nanoscale zerovalent iron particles

R.A. Crane[a,*], D.J. Sapsford[b]

[a] Camborne School of Mines, College of Engineering, Mathematics and Physical Sciences, University of Exeter, Penryn Campus, Penryn, Cornwall, TR10 9FE, United Kingdom
[b] School of Engineering, Cardiff University, Queen's Building, The Parade, Cardiff, CF24 3AA, United Kingdom

GRAPHICAL ABSTRACT

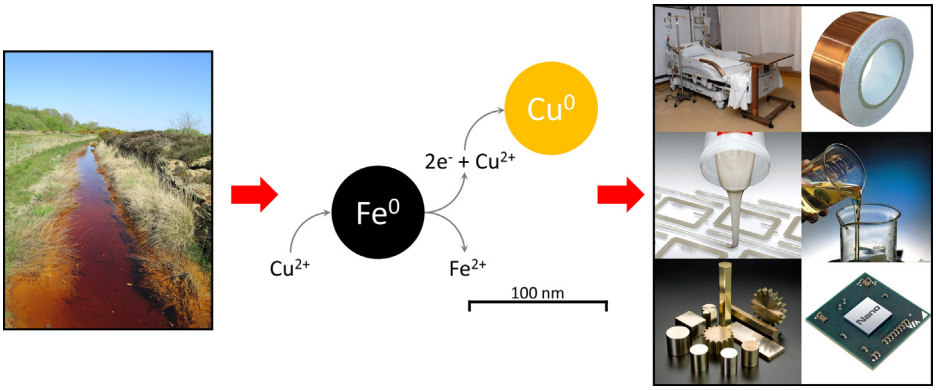

ARTICLE INFO

Article history:
Received 26 May 2017
Received in revised form 4 December 2017
Accepted 5 December 2017
Available online 18 December 2017

Keywords:
Nanoscale zerovalent iron particles
Copper
Cementation
Acid mine drainage
Aluminium

ABSTRACT

Nanoscale zerovalent iron (nZVI) has been investigated for the selective formation of Cu nanoparticles from acid mine drainage (AMD) taken from a legacy mine site in the UK. Batch experiments were conducted containing unbuffered (pH 2.67 at t = 0) and pH buffered (pH < 3.1) AMD which were exposed to nZVI at 0.1–2.0 g/L. Results demonstrate that nZVI is selective for Cu, Cd and Al removal (>99.9% removal of all metals within 1 h when nZVI ≥ 1.0 g/L) from unbuffered AMD despite the coexistent of numerous other metals in the AMD, namely: Na, Ca, Mg, K, Mn and Zn. An acidic pH buffer enabled similarly high Cu removal but maximum removal of only <1.5% and <0.5% Cd and Al respectively. HRTEM-EDS confirmed the formation of discrete spherical nanoparticles comprised of up to 68% wt. Cu, with a relatively narrow size distribution (typically 20–100 nm diameter). XPS confirmed such nanoparticles as containing Cu°, with the Cu removal mechanism therefore likely *via* cementation with Fe°. Overall the results demonstrate nZVI as effective for the one-pot and selective formation of Cu°-bearing nanoparticles from acidic wastewater, with the technique therefore potentially highly useful for the selective upcycling of dissolved Cu in wastewater into high value nanomaterials.

1. Introduction

Acid mine drainage (AMD) is an acidic solution that typically contains elevated concentrations of heavy metals and is caused by the microbial oxidation of pyrite and other sulphidic minerals, as

* Corresponding author.
E-mail address: r.crane@exeter.ac.uk (R.A. Crane).

https://doi.org/10.1016/j.jhazmat.2017.12.014

a consequence of the mining and processing of metal ores and/or coals [1,2]. Sulphidic minerals are extremely common and consequently many effluents derived from abandoned mines and mine wastes therefore exhibit a net acidity [1]. If left untreated AMD can contaminate ground and surface water and thereby damage ecosystems and potentially impact human health. As such the generation of AMD is often cited as one of the most prominent environmental issues currently facing the mining industry [1]. For example, in the UK alone it is estimated that as many as six percent of all surface water bodies are currently adversely affected by AMD derived from legacy metalliferous mines [3]. Similarly in the USA it is estimated that as many as 19,300 km of rivers and more than 180,000 acres of lakes and reservoirs have been damaged by AMD [4]. Consequently, the development of cost-effective remediation solutions for AMD has been the subject of intense research for several decades. Despite such interest, conventional AMD remediation technologies remain relatively expensive and/or require significant construction space (e.g. passive treatment), which poses a major challenge [1]. AMD often contains a wide range of metals and metalloids which while being toxic to the environment would also be beneficial to recover (e.g. Cu, Ni, Zn). Whilst it is possible to recover metals from dilute aqueous effluents using existing active treatment technologies e.g. ion exchange [1], the absence of widespread commercial practices for the recovery of metals from AMD indicates that the economic value of the metals rarely offsets the operating costs of recovery. As such a fundamental barrier exists where either the cost of AMD treatment needs to significantly decrease or the economically valuable metals present in such waste needs to be valorised into higher-value products, i.e. products which are worth significantly more than their raw metal value. With regard to the latter, one potential solution is to develop methodologies to *directly synthesise* high-value nanomaterials from AMD. Such nanomaterials could then be directly utilised as high value materials and/or reagents in a range of different processes, and as such provide significantly greater economic return than their equivalent bulk scale metal.

In recent years, nanoscale zero-valent iron (nZVI) has gained much attention for its use in a wide range of water treatment applications due to its unique properties, including high surface area to volume ratio and an ability to be injected into the subsurface as a colloidal suspension [5–8]. To date nZVI has been demonstrated as highly effective for the removal and/or degradation of a wide range of metals and metalloids (e.g. [7,9–17]), inorganic anions (e.g. [18]) and organic contaminants (e.g. [19–21]) from solution. Very little is known, however, with regard to the physicochemical properties of metals and metalloids when sorbed and/or chemically reduced by nZVI, and in particular whether such precipitates/particles could be recovered for economic gain. In particular almost all studies to date have investigated the use of nZVI for the sorption and/or enmeshment (i.e. the immobilisation) of metal and metalloid species. In contrast the use of nZVI for the *in situ* synthesis and recovery of functional (nano)materials from wastewater or contaminated land is a new research arena. Preliminary evidence has already been presented on the formation of iron-bearing nanomaterials from AMD [22], however, to the best of our knowledge no studies have yet investigated the selective formation of heavy metal (e.g. Cu, Zn, Al) nanomaterials from AMD.

It is well known that nZVI is highly efficient for the removal of aqueous Cu under a range of different chemical conditions (e.g. [10,23] and [24]), however, the extent at which nZVI might be selective for the removal of aqueous Cu from wastewater (such as AMD) remains unknown. Furthermore very little is known with regard to the physico-chemical properties of such recovered Cu, such as whether, and if so under what conditions, discrete Cu-bearing nanoparticles might form due to the cementation reaction between aqueous Cu and Fe°. This study has been established in order to investigate these phenomena in order to gain an understanding of the extent at which nZVI could be used for the selective formation of Cu-bearing nanoparticles from AMD which could prove a highly useful mechanism for the valorisation of Cu-bearing AMD, thereby unlocking a new economic incentive for AMD treatment. Such novel approaches are urgently required from addressing AMD which is one of the most prominent environmental issues currently facing the mining industry, and regarded by the European Environment Bureau and the US Environmental Protection Agency and as "second only to global warming and stratospheric ozone depletion in terms of global ecological risk" [25].

2. Methodology

2.1. AMD sampling location

The AMD used in this study was collected from Parys Mountain which is a disused open cast Cu-Pb-Zn mine on Anglesey (Wales, UK) [26]. Samples were collected from the Duffryn Adda adit (GPS location: 53°23′40.96 N, 4°21′01.80 W) and sealed in high-density polyethylene bottles (without headspace) and stored at 4 °C until required (maximum storage time was 7 days). The AMD initially contains low concentrations of dissolved oxygen (DO), (e.g. <2 mg/L), however, it quickly equilibrates with the atmosphere when in surface waters to reach oxygen concentrations more typical for that of vadose and/or surface waters (e.g. ~7–10 mg/L), changing its redox potential and associated heavy metal transport properties in the process.

2.2. Zero-valent iron nanoparticle synthesis

Pure nZVI were synthesised following the methodology first described by Glavee et al., [27] and then adapted by Wang and Zhang [28]. 7.65 g of $FeSO_4{\cdot}7H_2O$ was dissolved in 50 mL of Milli-Q water (>18.2 MΩ cm) and the pH was adjusted to 6.8 using 4 M NaOH. NaOH addition was performed slowly, drop-wise, to avoid the formation of hydroxo-carbonyl complexes. The salts were reduced to nZVI by the addition of 3.0 g of $NaBH_4$. The nanoparticle product was isolated from the aqueous phase via centrifugation (Hamilton Bell v6500 Vanguard centrifuge, 6500 rpm for 120 s), rinsed with absolute ethanol (Fisher Scientific, 12478730; ratio of 50 mL/g of nZVI) and then centrifuged (Hamilton Bell v6500 Vanguard centrifuge, 6500 rpm for 120 s). This step was then repeated three more times. The nanoparticles were dried in a vacuum desiccator (approx. 10^{-2} mbar) for 72 h and then stored in an argon filled (BOC, 99.998%) MBraun glovebox until required.

2.3. Exposure of nZVI to the AMD

Prior to conducting any nZVI-AMD exposure experiments the AMD was removed from the refrigerator and allowed to equilibrate in the ambient laboratory (temperature = 20.0 ± 1.0 °C) for 24 h. Unless specified differently all batch systems comprised 200 mL volume of the AMD in 250 mL clear soda lime glass jars. Following nZVI addition the batch systems were immediately sonicated for 120 s using an ultrasonic bath (Grant, XB3). Each system was then sealed (using a screw cap) and placed on the benchtop in the open laboratory. Periodic sampling of dissolved oxygen (DO), oxidation reduction potential (ORP) and pH was conducted by gently agitating each batch system in order to ensure homogeneity. The pH, Eh and DO probes were calibrated prior to each measurement. The measured Eh values were converted to Eh (vs. standard hydrogen electrode) by subtracting the difference between the measured Eh of the reference solution (220 ± 5 mV) with the true Eh of the reference solution (Mettler Toledo 220 mV/pH 7 reference solution). 5 mL aqueous-nZVI suspensions were periodically taken using an auto-pipette. The extracted suspensions were centrifuged

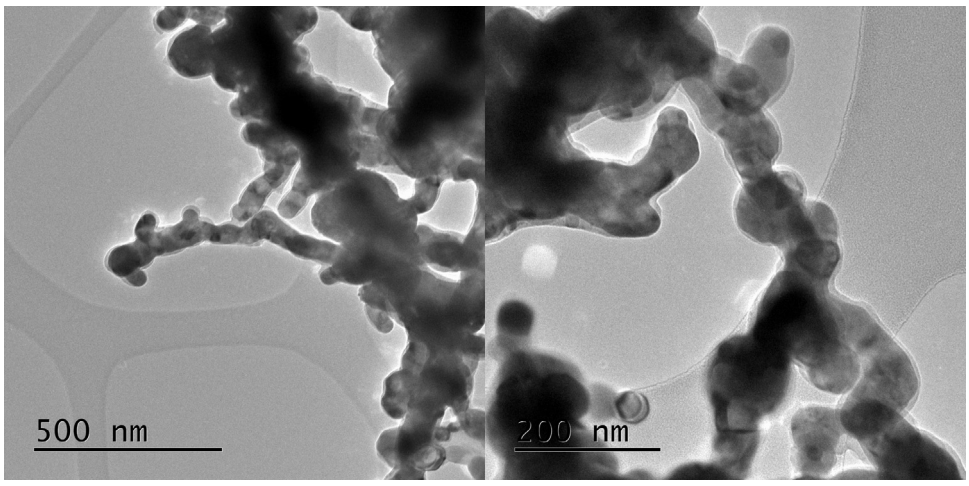

Fig. 1. HRTEM images of the as-formed nZVI.

at 4000 rpm (3077 *g*) for 240 s after which the supernatant became clear (i.e. all of the nZVI was centrifuged to the bottom of the vial). The supernatant was then extracted using a 10 mL syringe and filtered through a cellulose acetate filter 0.2 μm filter. The filtered water was prepared for inductively coupled optical emission spectrometry (ICP-OES) by the additional of HNO_3 at a concentration of 2% by volume. The solid nZVI plug at the base of each centrifuge vial was prepared for X-ray diffraction (XRD), X-ray photoelectron spectroscopy (XPS) and high resolution transmission electron microscopy (HRTEM) by an absolute ethanol wash. This was conducted by adding 20 mL of ethanol (Fisher Scientific, 12,478,730) and then gently agitating the centrifuge vial in order to suspend the nZVI plug. The vial was then centrifuged at 4000 rpm (3077 *g*) for 240 s in order to separate the solid and aqueous phases. The supernatant was then removed and the process was repeated a further two times. Each time the supernatant was decanted the nZVI plug at the bottom of the centrifuge vial was maintained in place using an Eclipse 20mm Neodymium Pot Magnet (length 25mm, pull force 28kg). Once the ethanol washing process was completed the nZVI plug was pipetted onto a glass optical microscope slide (Agar Scientific, G251P) for XRD and XPS analysis and a Au coated holey carbon film (TAAB, C062/G) for HRTEM analysis. Samples were then dried in a vacuum chamber at $<1 \times 10^{-2}$ mbar for a minimum of 2 h prior to analysis. In order to test the influence of a constant pH on the metal/metalloid removal behaviour from the AMD onto nZVI pH buffered batch systems were created. 180 mL of the AMD was first added to two different 250mL clear soda lime glass jars. 20 mL solutions of 0.05 M or 0.1 M HCl with both containing 1.0 g of potassium hydrogen phthalate ($C_8H_5KO_4$) was then added to each of the batch systems. The solutions were then gently stirred and left for 24 h to equilibrate prior to nZVI addition. Sorption-desorption experiments were then conducted following the same methodology outlined above. In order to test the reusability of nZVI for the removal of metal/metalloids from the AMD the nZVI were exposed to the AMD (40 mL of AMD and nZVI at 1g/L) inside 50 mL centrifuge vials. The batch systems were first sonicated using an ultrasonic bath (Grant, XB3) for 120 s and then left for 30 min. The batch systems were then centrifuged at 4000 rpm (3077 *g*) for 240 s. The supernatant was then filtered through a cellulose acetate filter 0.2 μm filter and prepared for ICP-OES analysis following the technique described above. The nZVI plug at the bottom of the centrifuge vial was maintained in place using an Eclipse 20mm Neodymium Pot Magnet (length 25mm, pull force 28kg) and the remaining supernatant was decanted. 40 mL of fresh AMD was then added and the steps listed above were repeated six times. All sorption-desorption experiments were conducted at room temperature (measured to be 20.0 °C ±1.0 °C) and ran as duplicate pairs, with the average data used to create the figures/tables displayed herein.

2.4. Analytical techniques

A Phillips Xpert Pro diffractometer with a CoKa radiation source was used for XRD analysis (generator voltage of 40 keV; tube current of 30 mA). XRD spectra were acquired between 2h angles of 10–90°, with a step size of 0.02° 2 and a 2 s dwell time. ICP-OES analysis of aqueous samples was performed using a PerkinElmer Optima 2100 DV ICP-OES. HRTEM analysis was performed using a JEOL JEM-2100 microscope at 200 kV. Energy dispersive spectroscopy (EDS) analysis and mapping was performed using Oxford Instruments X-MaxN analyzer and Aztec software. A beryllium sample holder was used in order to prevent any background Cu from being detected. Nanoparticle size distribution from HRTEM images was measured using ImageJ software (Java 1.6.0_24) with 50 nanoparticles analysed per sample. X-ray photoelectron spectroscopy (XPS) spectra were collected using a Thermo K-Alpha+ spectrometer. Spectra were collected at a pass energy of 40 eV for narrow scans and 150 eV for survey scans with a 0.1 and 1 eV step respectively. Charge neutralisation was achieved using a combination of low energy electrons and argon ions. Spectra were quantified in CasaXPS using Scofield sensitivity factors and an energy dependence of -0.6. In order to determine the relative proportions of Fe^{2+} and Fe^{3+} in the sample analysis volume, curve fitting of the recorded Fe $2p_{3/2}$ photoelectron peaks was performed following the method of Scott et al. [29]. The Fe $2p_{3/2}$ profile was fitted using photoelectron peaks at 706.7, 709.1, 710.6 and 713.4 eV corresponding to Fe°, Fe^{2+} octahedral; Fe^{3+} octahedral and Fe^{3+} tetrahedral. These parameters were selected on the basis that the surface oxide was assumed to be a mixture of wüstite and magnetite, as the oxide Fe^{2+} is in the same coordination with the surrounding oxygen atoms in both forms of oxide.

3. Results and discussion

3.1. Characterisation of the as-formed nZVI

Characterisation of the as-formed nZVI was performed using BET surface area analysis, HRTEM, XRD and XPS. BET surface area analysis determined that the surface area of the nZVI was 50.9 m^2/g. HRTEM analysis determined that the nZVI were spherical, generally

Table 1
Summary of the physicochemical properties of the as-formed nZVI.

Parameter	Analysis technique	nZVI
Particle size distribution (%)	HRTEM	0–50 nm: 32.1 50–100 nm: 58.5 > 100 nm: 9.4
Bulk composition	XRD	α-Fe°
Oxide thickness (nm)	HRTEM, XPS	3-5
Surface composition (at. %)	XPS	Fe: 19.1 O: 52.4 C: 5.0 B: 15.7 Na: 7.8
Fe stoichiometry ($Fe^{\circ}/Fe^{2+}+Fe^{3+}$)	XPS	0.19
Specific surface area (m^2/g)	BET	50.9

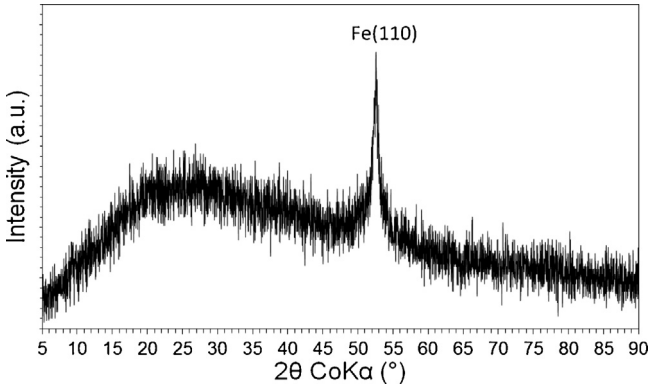

Fig. 2. XRD spectra for the as-formed nZVI.

within a size range of 10–150 nm and an average diameter of 61 nm (Fig. 1). Each individual nZVI particle was recorded to contain a discrete outermost layer (density contrast), which is attributed to be the presence of an oxide shell surrounding the Fe° core. In addition dark mottles were recorded within the metallic cores which indicates that individual particles are either polycrystalline or comprised isolated metal crystals in an otherwise amorphous matrix. Individual nZVI particles were aggregated into chains and rings due to their high surface energy and magnetic properties [30]. A single diffraction peak at 52.381° 2θ was recorded using XRD and attributed to the (110) lattice reflection of α-Fe° (Fig. 2). The peak was relatively broad which indicates that the nZVI are relatively amorphous. XPS analysis determined the outer surface of the nZVI is comprised of a mixed valent (Fe^{2+}/Fe^{3+}) oxide overlying a Fe° core. Given the mean free path of Fe is equivalent to approximately 6 atomic layers, this detection of Fe° in the XPS analysis volume therefore indicates that the oxide thickness is likely to be <5nm, which corroborates the aforementioned nZVI oxide thickness measurement using HRTEM. The results are summarised in Table 1.

3.2. Characterisation of the AMD

Prior to nZVI addition the pH, Eh and DO of the AMD was measured along with the concentrations of dissolved metals and metalloids using ICP-OES. The water was acidic (pH = 2.67) and oxygen-rich (DO and Eh 395 mV and 8.98 mg/L respectively). In order to highlight the highly polluted nature of the water, concentrations of notable metal and metalloids present in the AMD are presented along with their World Health Organisation (WHO) recommended drinking water human health guideline concentrations [31] in Table 2, and were used throughout this paper as reference conditions. Several elements were recorded as exceeding the guideline concentrations, namely Mn, Ni, Cu and Cd by factors of 44.8, 1.9, 22.7 and 56.7 respectively. The concentrations of all metals and metalloids analysed using ICP-OES is displayed in Table S1.

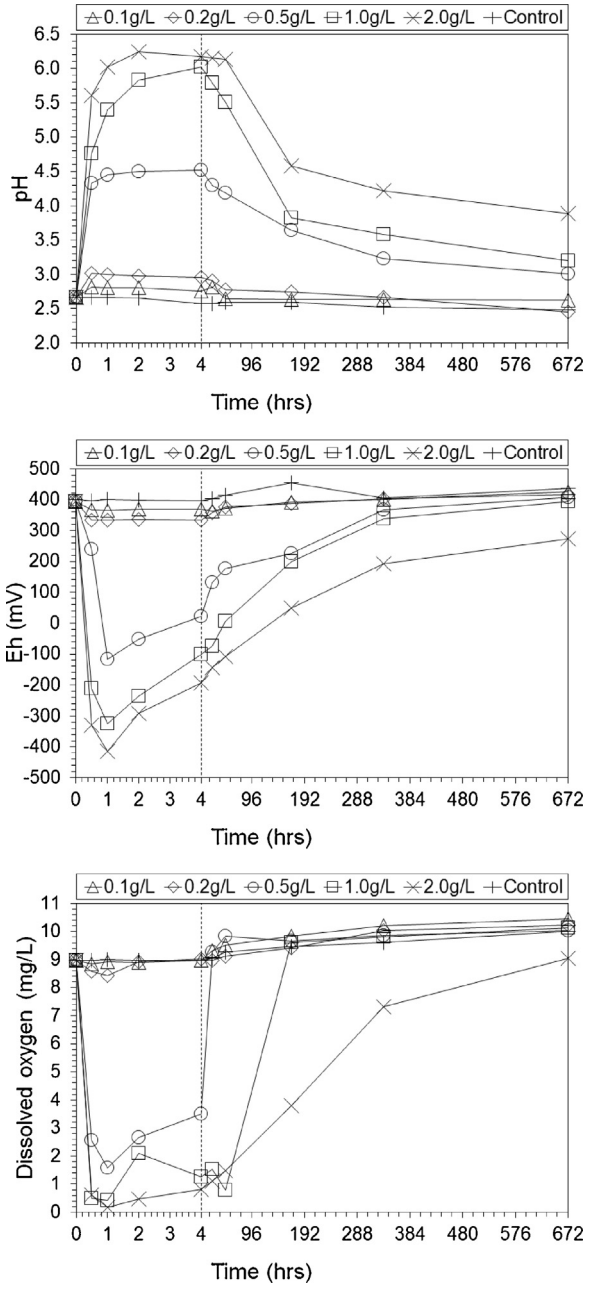

Fig. 3. Changes in pH, Eh and DO as a function of time for the unbuffered batch systems.

3.3. Changes in pH, Eh and DO

The addition of the nZVI to all batch systems containing AMD (no pH buffer) resulted in a rapid decrease in Eh and DO and a concurrent increase in pH (Fig. 3). Most significant change was recorded for the batch systems containing the largest concentration of nZVI

Table 2
Notable contaminant metal and metalloids present in the AMD along with their WHO recommended drinking water health guideline concentrations [31]. Metal/metalloid concentrations of the unbuffered AMD following exposure to nZVI (2 g/L concentration) for 1hr and 28 d are also listed. Cells are coloured in red where metal/metalloid concentrations exceed the WHO threshold. (For interpretation of the references to colour in this table, the reader is referred to the web version of this article.)

Metal/metalloid	Concentration in AMD (mg/L)	WHO drinking water guideline concentrations (mg/L)	Concentration after 1hr (nZVI at 2 g/L)	Concentration after 28d (nZVI at 2 g/L)
B	0.55	2.4	46.03	105.99
Na	15.91	No limit	41.07	47.08
Mg	108.90	No limit	112.49	118.85
Al	77.69	No limit	<DL	27.00
K	2.36	No limit	2.85	2.13
Ca	69.49	No limit	72.51	83.12
Mn	17.93	0.4	17.08	17.48
Fe	592.80	No limit	1058.80	813.62
Ni	0.13	0.07	0.05	0.11
Cu	45.41	2	<DL	33.48
Zn	70.49	No limit	55.18	72.22
Cd	0.17	0.003	<DL	0.16

with only relatively minor changes recorded for the batch systems containing nZVI at <0.5 g/L. Eh minima were recorded for the AMD exposed to nZVI at concentrations of 0.2, 0.5, 1.0 and 2.0 g/L within the first 1 h of reaction, with 428, -21, −231 and −319 mV respectively recorded. In contrast an Eh minimum of 457 mV was recorded after 24 h exposure of the AMD to nZVI at 0.1 g/L. The Eh in all systems was 395 mV at t = 0. Maxima in pH were recorded within the first four hours of exposure of the AMD to nZVI at concentrations of 0.2, 0.5, 1.0 and 2.0 g/L, with 3.02, 4.52, 6.02 and 6.24 recorded respectively. In contrast a pH maximum of 2.82 was not recorded until after 24 h exposure of the AMD to 0.1 g/L nZVI. The pH was 2.67 at t = 0 in all systems. Such redox and pH changes are attributed to the rapid oxidation of nanoparticulate surfaces during their initial exposure to the AMD, consuming DO and H^+ and reducing the Eh of the system. Following this initial reaction period gradual reversal to ambient pH, Eh and DO conditions was observed for all systems, which is attributed to the reactive exhaustion of the nZVI (i.e. total transformation of Fe° to Fe^{3+} (hydr)oxide products). Changes in pH, Eh and DO recorded following exposure of the nZVI to the pH buffered AMD is displayed in Fig. S1. It can be observed that similar changes in Eh and DO occurred when compared to the unbuffered AMD, however, only a minor increase in pH was recorded, with maxima of 2.30 and 3.09 recorded after 24 h for the batch systems containing buffer reagents 0.1 g/L $C_8H_5KO_4$ and 0.01M HCl 0.1 g/L and 0.1 g/L $C_8H_5KO_4$ and 0.005M HCl respectively (pH was 1.91 and 2.42 at t = 0 respectively). Figure S2 displays pH, Eh and DO changes for AMD when fresh AMD was added to the nZVI every 30 min. Similar changes in pH, Eh and DO were observed for the first two exposures, however, after the third exposure of the nZVI to the AMD a clear return to ambient electrochemical conditions was recorded and attributed to the reactive exhaustion of the nZVI. This was corroborated visually; the batch systems eventually became clear due to the total dissolution of the nZVI into the AMD.

3.4. Changes in aqueous metal concentrations

3.4.1. Metal/metalloid removal onto nZVI

The addition of the nZVI to the AMD (no pH buffer) resulted in significant changes in the aqueous concentration of several different metals and metalloids (Fig. 4 and Table 2). The most significant concentration decreases were recorded for Cu, Al and Cd with removal of these metals to below ICP-OES detection limits (after 10X dilution) recorded within 2 h reaction time when using nZVI concentrations of ≥ 1 g/L, followed by retention below WHO specified drinking water guideline concentrations (Table 2) for time periods ≥24 h. A decrease in the concentrations of Zn and Ni was also recorded but at a lower magnitude (both in terms of relative quantities removed and the duration of removal). The Zn concentration minimum was 14.9 mg/L (nZVI concentration: 2 g/L, sampling time: 48 h), or 78.8% removal. However, Zn removal of <50% was recorded for all other sampling times with the exception of the 24 h sampling time (when using a nZVI concentration of 2 g/L), where removal of 72.0% was determined. Removal of Ni to below WHO specified drinking water guideline concentrations was recorded throughout the entire reaction period except the 28 d sampling time for the batch system containing nZVI at a concentration of 2 g/L, however, removal of only <50% was typically recorded for all other nZVI concentrations. Minimal concentration changes were recorded for major cations: Ca, Mg, K and Mn (Table 2) which demonstrates that nZVI is selective for the removal of certain metals from solution (namely those whose solubility is redox sensitive). It has been reported that the removal mechanism of metals and metalloids by nZVI is typically *via* adsorption/surface complexation for metal ions which have the standard electrode potentials (E°) for reduction to a metallic state that are very close to, or more negative than Fe° (-0.44 V), such as Zn^{2+}. Moreover, for metal ions such as Cu^{2+} which have a E° that is much more positive than Fe°, removal is typically via surface-mediated cementation [7], Eq. (1).

$$Fe^\circ + Cu^{2+} = Fe^{2+} + Cu^\circ \quad E^\circ = 0.78 \tag{1}$$

Metal cations such as Ni^{2+} which are only slightly more electropositive than Fe° are typically removed from solution *via* a combination of adsorption and (partial) chemical reduction. The E° for the cathodic reduction of aqueous K^+, Ca^{2+}, Na^+, Mg^{2+} and Mn^{2+} to their metallic state is −2.92, −2.84, −2.71, −2.37 and −1.18 V respectively. The lack of removal from solution of such ions onto nZVI is therefore likely to be due to their more negative E° (for reduction to a metallic state) than Fe°. Significant removal of Al onto nZVI was recorded, however, despite the $E0$ for the cathodic reduction of aqueous Al^{3+} to its metallic state being −1.66 V, and therefore considerably lower than −0.44 V. However, within the pH range of approximately 4–8 Al is known to readily precipitate from solution as a hydroxide, namely gibbsite ($Al(OH)_3$) [32]. Similarly, the $E0$ for the cathodic reduction of aqueous Zn^{2+} and Cd^{2+} to their metallic state are −0.76 and −0.40 V respectively and as such their removal by nZVI recorded herein is likely also to be due to the

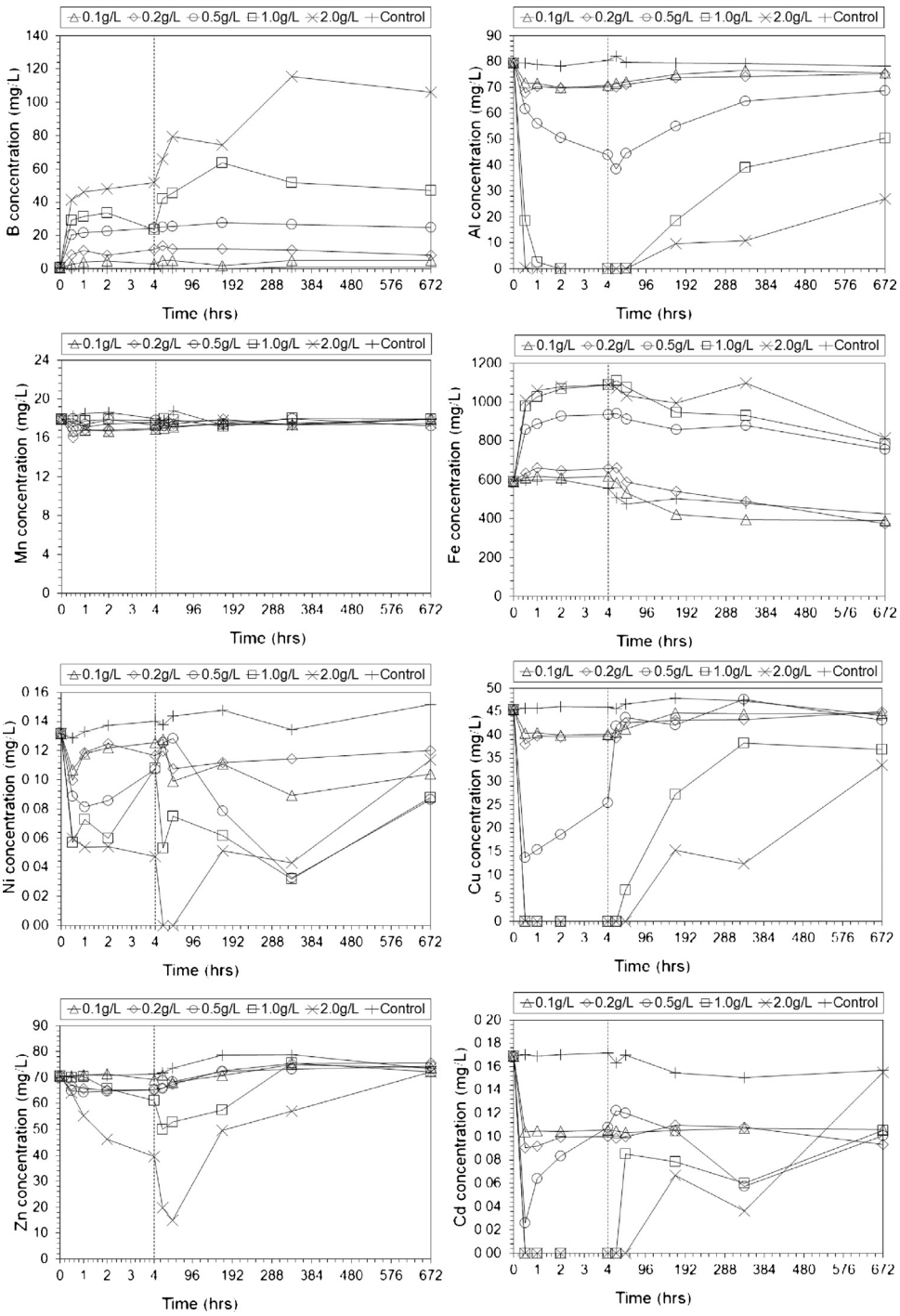

Fig. 4. Aqueous concentrations of notable metal and metalloids as a function of time for the AMD when exposed to nZVI at 0.1, 0.2, 0.5, 1.0 and 2.0 g/L.

pH increase, resulting in the co-precipitation (and adsorption) of Zn and Cd with nZVI corrosion products and/or iron (hydr)oxides derived from native iron within the AMD [32]. In contrast to other metal/metalloids the concentrations of Fe, Na and B were recorded to increase in all batch systems, with a relatively linear correlation with the mass of nZVI added observed, and as such their behaviour is attributed to the dissolution of such metals from the nZVI, with Na and B likely to have been derived from the $NaBH_4$ used in the nZVI synthesis.

Fig. 5 displays dissolved metal concentration data as a function of time for the pH buffered AMD following exposure to the nZVI at a 1.0 g/L concentration. It can be observed that in contrast to the unbuffered AMD system (Fig. 4) no appreciable removal of Al, Zn or Cd was recorded, which is attributed to the increased solubility of such metals at the lower pH [32].

Fig. 6 displays changes in the concentration of notable dissolved metals as a function of time for the AMD when fresh AMD was added to the nZVI every 30 min. Results demonstrate that under such conditions nZVI was least able to retain Al (desorption occurred upon the second exposure to the AMD) followed by Cu, Ni and Cd (desorption of such metals occurred upon the third exposure to the AMD). In contrast removal of >20% of dissolved Zn was recorded in all instances, which suggests that the nZVI are suitable to be reused for Zn removal from solution. Fe and B concentrations were

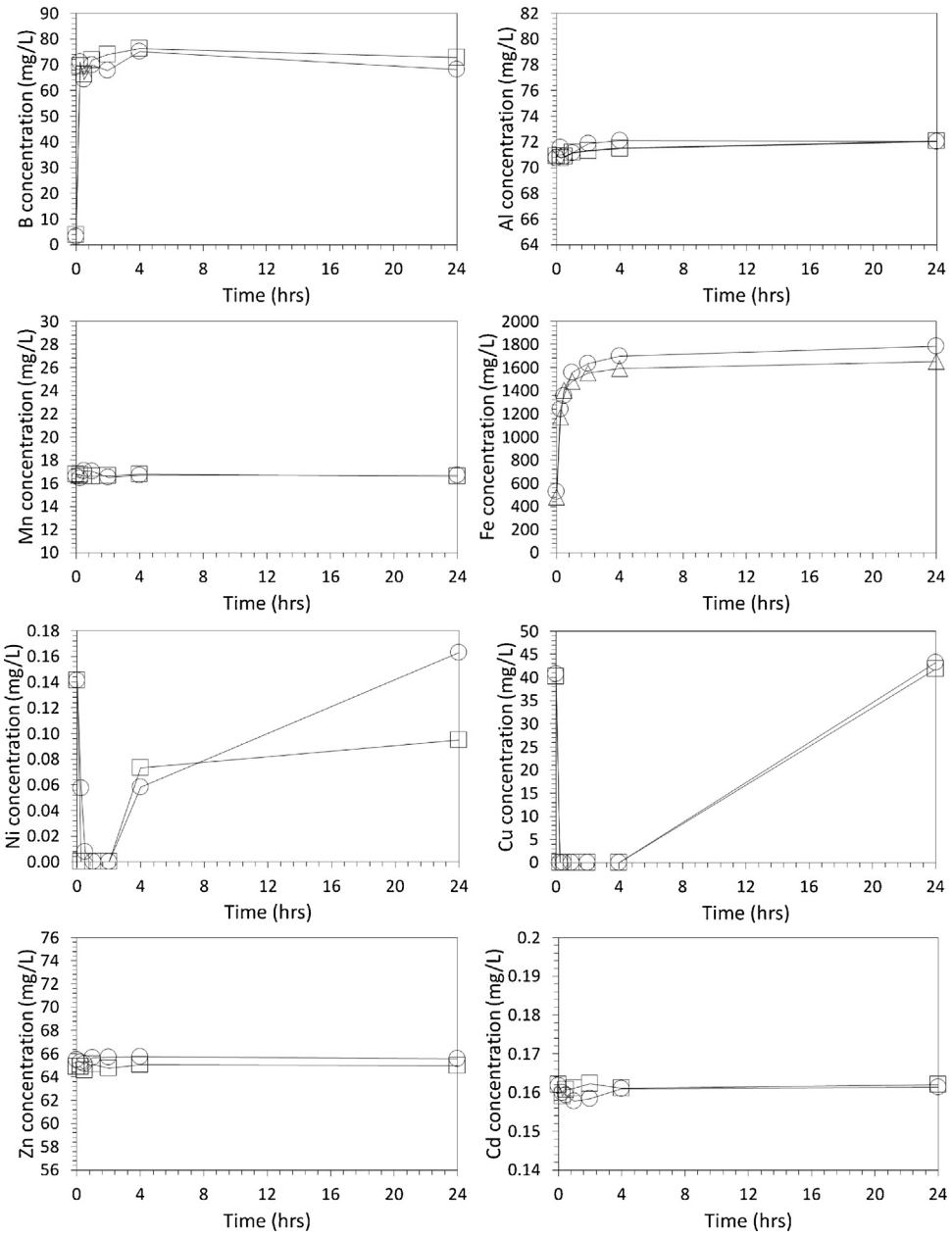

Fig. 5. Changes in the aqueous concentration of notable metal and metalloids as a function of time for the pH buffered AMD following exposure to the nZVI at a 1.0 g/L concentration. Square and circle markers denote systems with buffer reagents comprising of 0.1 g/L $C_8H_5KO_4$ and 0.005M HCl and 0.1 g/L $C_8H_5KO_4$ and 0.01M HCl respectively.

recorded to initially increase and then decrease in the latter stages of the experiment. This is attributed to the dissolution of the nZVI into the acidic AMD which was also observed visually: the nZVI suspensions became progressively clearer due to the progressive and eventually total dissolution of the nZVI into the AMD.

3.4.2. Metal/metalloid rerelease

It can be observed in Table 2 and Fig. 4 that following their initial removal from the aqueous phase significant release of heavy metals (namely Al, Zn, Ni and Cd) was recorded in all systems. This behaviour is in agreement with other studies (e.g. [33]) and was coincident with the reactive exhaustion of the nZVI and consequent reversal of the solution chemistry to pre-nZVI addition conditions, resulting in a combination of dissolution and desorption of metals from corrosion products as pH reverted to lower values and Eh increased in response to atmospheric oxygen ingress. The redissolution of Cu was recorded to commonly occur in the latter stages of the exposure of nZVI to both unbuffered and pH buffered AMD and probably resulted from the oxidative dissolution of Cu° to Cu^{2+} as Eh climbed above ~200 mV. XPS observations (see Section 3.5.2.) provide further evidence of this mechanism. This behaviour provides clear evidence that nZVI is only suitable for the recovery of Cu from DO-bearing AMD over relatively short time periods (e.g. <48 h), with the recovery of nZVI (and cemented Cu) necessary within such a time period, unless either favourably low Eh can be maintained or pH can be buffered to remain circumneutral or basic. Interesting this phenomena could potentially be harnessed as a new method to concentrate Cu whereby following the selective recovery of Cu from the AMD the nZVI (and sorbed Cu) could then be separated into a smaller volume of AMD (e.g. *via* centrifugation or coagulation/flocculation) with the Cu then allowed to be release back into the aqueous phase, thus concentrating the Cu for final recovery.

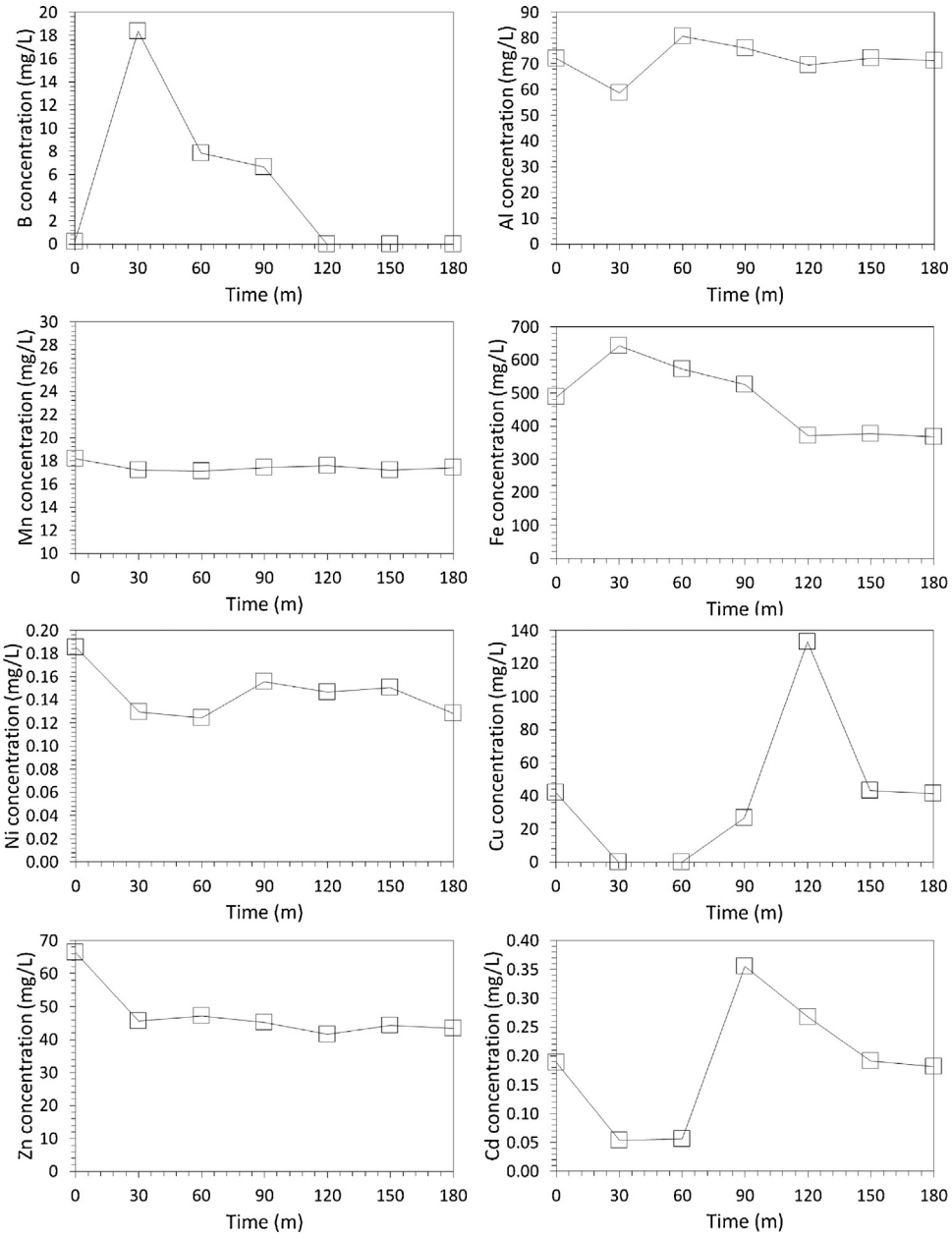

Fig. 6. Changes in the aqueous concentration of notable metal and metalloids as a function of time for the AMD when fresh AMD has been used every 30 min. A nZVI concentration of 1.0 g/L was used.

3.5. Physicochemical properties of nanoparticulate products

3.5.1. XRD data

XRD was used to determine the bulk crystallinity and composition of nZVI solids extracted from all batch systems at periodic time intervals during their exposure to the AMD (Fig. S3). A transition from Fe°, with a well-defined peak centred at 52.6° 2θ (lattice reflection: Fe(110)), to a broad (and low intensity) peak centred at approximately 25° 2θ was recorded for all systems, indicating the formation of an amorphous iron hydroxide phase. In systems containing nZVI at concentrations of 0.1–1.0 g/L Fe° was not detected at the first sampling time of 30 min. In contrast Fe° was detected until 24 h for the system containing nZVI at 2.0 g/L. In all systems the amorphous iron hydroxide phase remained until the end of the 28 d reaction period, however, goethite (α-FeOOH) emerged after 7 d reaction for the batch system containing nZVI at 2.0 g/L, with greatest intensity peaks centred at 24.6, 38.8, 42.8, 46.9, 48.2 and 62.6° 2θ recorded corresponding to lattice reflections of 110, 130, 111, 210, 140 and 221 respectively. Goethite continued to crystallize into the latter stages of the experiment to become the sole crystalline corrosion product after 28 d. However, the intensity of the goethite peaks remained relatively low. This was not unexpected given that the transformation of amorphous iron hydroxides to goethite can be efficiently retarded by the presence of co-precipitated Al [34]. XRD spectra recorded for nZVI extracted from the pH buffered AMD is displayed in Fig. S4. It can be observed that, similar to the unbuffered system, a transition from Fe°, with a well-defined peak centred at 52.6° 2θ (lattice reflection: Fe(110)), to a broad (and low intensity) peak centred at approximately 25° 2θ was recorded and attributed to the formation of amorphous iron hydroxide.

3.5.2. XPS data

XPS was used to characterise the surface chemistry of nZVI following exposure to the unbuffered and pH buffered AMD includ-

Table 3
Concentration of Al, C, Cu, Fe, O and Zn (at. %) determined using XPS analysis of solid samples extracted from the batch system containing the AMD and nZVI at 1.0 g/L. Al, C, Cu, Fe, O and Zn data are determined by integrating the area under the Al 2p, C 1s, Cu 2p3/2, Fe 2p3/2, O 1s and Zn 2p 3/2 photoelectron peaks respectively. *The majority of C detected is likely to be comprised of adventitious carbon. Corresponding data for the as-formed nZVI can be found in Table 1. **The pH buffer reagents comprised 0.1 g/L $C_8H_5KO_4$ and 0.005M HCl.

Time (hrs)	Al	C*	Cu	Fe	O	Zn
Unbuffered AMD						
0.5	11.44	10.84	2.60	5.01	69.94	0.17
1	9.45	10.71	2.79	6.93	69.85	0.27
2	8.00	11.44	2.46	7.74	69.71	0.65
4	8.91	11.44	2.35	6.90	69.47	0.93
24	7.29	8.85	2.57	6.01	73.5	1.78
48	10.13	7.77	2.37	5.31	72.94	1.48
168	8.53	9.41	0.00	7.49	74.43	0.14
336	4.60	10.72	0.00	10.01	74.45	0.22
672	1.89	8.56	0.00	11.33	78.22	0.00
pH buffered AMD**						
1	0.94	19.31	0.24	5.78	73.73	0.00
2	1.23	12.43	0.29	2.10	83.95	0.00
4	0.00	33.34	3.18	17.36	46.12	0.00
24	0.00	33.36	6.60	17.25	42.79	0.00

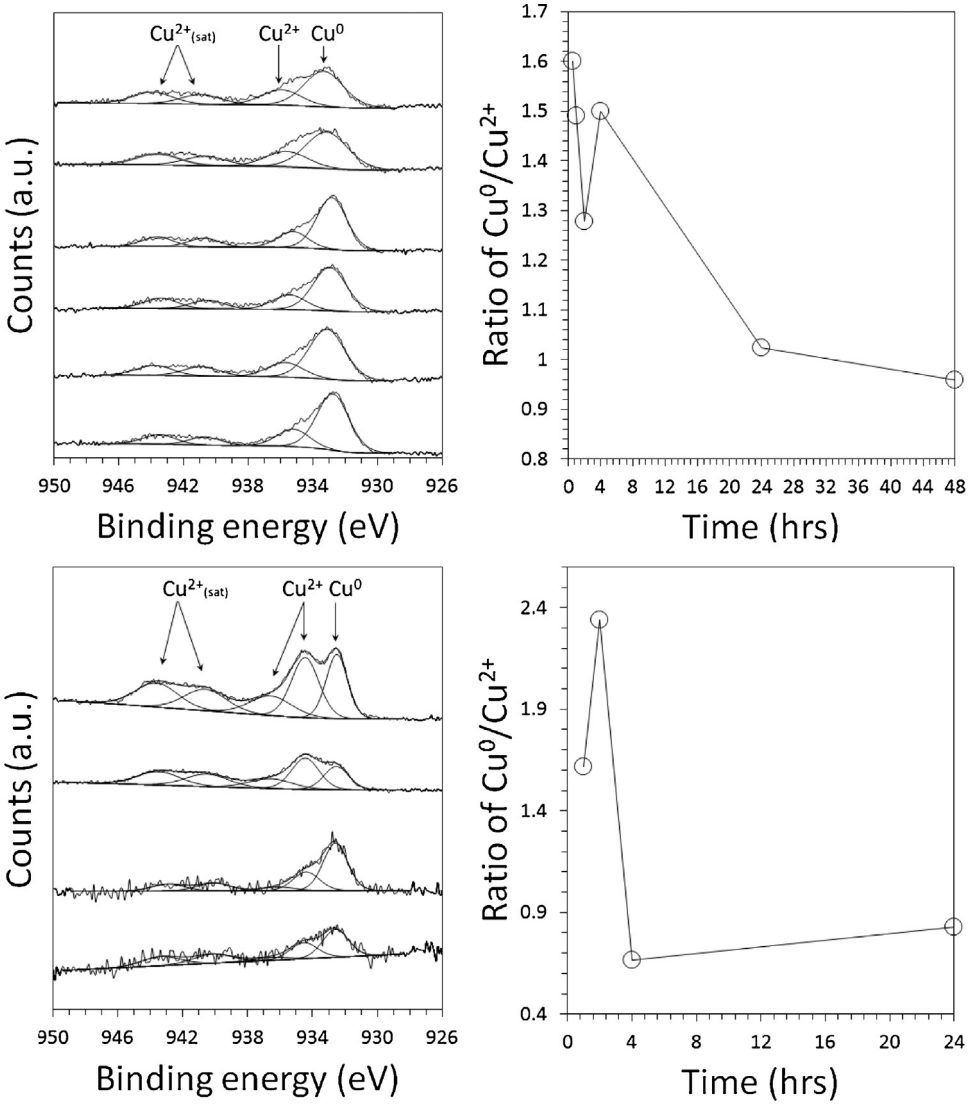

Fig. 7. Curve fitted XPS Cu $2p_{3/2}$ spectra for nZVI extracted from the unbuffered (top) and pH buffered* (bottom) AMD after 0.5, 1, 2, 4, 24 and 48 h and 1, 2, 4 and 24 h (stacked from bottom to top) respectively along with corresponding ratios of Cu°/Cu^{2+} calculated by integrating the area under each corresponding curve fitted photoelectron peak. A nZVI concentration of 1.0 g/L was used. *The pH buffer reagents comprised 0.1 g/L $C_8H_5KO_4$ and 0.005M HCl.

ing any sorbed or cemented species (Table 3 and Fig. 7). Fe$2p_{3/2}$ photoelectron peaks recorded for unreacted nZVI confirmed the outermost surface of the nanomaterial to be a mixed valence oxide, with a Fe$2p_{3/2}$ peak centred at 710.9 eV (Section 3.1). Fe° was also

detected, which as discussed in Section 3.1., indicates that the oxide thickness of the as-formed nZVI is likely to be <5nm. Subsequent XPS analysis of nZVI extracted from both unbuffered and pH buffered AMD at periodic time intervals determined a slight shift in the location of the $Fe2p_{3/2}$ peak to between approximately 711.1 and 711.5 eV for nZVI extracted after time periods ≤1 h (Fig. S5). This was then maintained at approximately ± 0.2 eV for the entire reaction period. In addition Fe° was not detected in any samples. This provides clear evidence that the entire mass of Fe° located in the outer ~5 nm of each nZVI was oxidised (to Fe^{2+}) within 30 m of exposure to the AMD (i.e. the oxidation was rapid and did not leave behind any regions of unoxidised Fe°).

O1s spectra recorded for the unreacted nZVI (Fig. S5) confirmed that the outmost surface was a mixture of metal oxide (binding energy 529–531 eV) with a small component of surface hydroxyl (binding energy 530-532 eV) and H_2O (binding energy (531–533 eV), which agrees with previous studies (e.g. [8]). Following exposure of the nZVI to the AMD a decrease in the proportion of metal oxide photoelectron peaks relative to hydroxyl and H_2O was recorded and attributed to the oxidation of nZVI surfaces and consummate sorption of H_2O and formation of metal hydroxide phases.

Al_{2p} spectra (only detected for the nZVI following exposure to the unbuffered AMD) were centred at binding energies of ranging from 74.4 to 74.9 eV (mean = 74.7 eV) with no shoulder peak(s) recorded at 72.7 ± 0.2 eV. XPS spectra for Al oxides and hydroxides are known to overlap each other [35] and as such differentiation between such phases was not possible, however, this result indicates that Al° was not present (Al° is typically recorded at a binding energy of 72.7 ± 0.1 eV) [35]. No clear change in the Al_{2p} photoelectron peak shape or binding energy was recorded as a function of time for the samples indicating that no change in the composition of sorbed or precipitated Al occurred.

$Cu2p_{3/2}$ spectra were asymmetric, with curve fitting yielding two or three photoelectron peaks centred at binding energy ranges of 932.8–933.3 eV (mean = 933.0 eV) and 935.2-935.9 eV (mean = 935.5 eV) along with two shake-up satellites centred within the range of 940.5-940.9 eV (mean = 940.8 eV) and 943.4-943.9 eV (mean = 943.6 eV), Fig. 6. Cu° and Cu^+ are typically cited as exhibiting XPS $Cu2p_{3/2}$ spectra centred at binding energies of 932.6 and 932.4, however, an additional shake-up satellite centred at approximately 945.0 eV is also typically indicative of the latter specie (in the form of Cu_2O) [36]. Tetrahedral and octahedral Cu^{2+} is typically cited as exhibiting a photoelectron peak at approximately 933.6 and 934.0 eV respectively along with shake-up satellites centred at approximately 940.8 and 943.6 eV [37]. It is therefore likely that the Cu was likely present as a mixture of Cu° and octahedral Cu^{2+}, with the former species likely formed via cementation with Fe° from the nZVI (Eq. (1)). The presence of octahedral (rather than tetrahedral) Cu^{2+} indicates that it was perhaps incorporated into the nZVI structure via substitution upon octahedral sites, such as spinel (e.g. magnetite) [37]. A clear decrease in the proportion of Cu° relative to Cu^{2+} was recorded as a function of time for the nZVI when exposed to the AMD (Fig. 6). This coincides with the significant release of Cu which was recorded using ICP-OES (Fig. 4), which therefore indicates that such Cu release is likely to be related to Cu° reoxidation.

Table 3 displays the surface concentration of different elements (at.%) determined using XPS analysis of the nZVI extracted at periodic time intervals following exposure to the AMD. Following the addition of the nZVI to the AMD an increase in the proportion of O and a commensurate decrease in the proportion of Fe was recorded and attributed to the build-up of nZVI corrosion phases at the surface of the nanomaterial. Appreciable surface concentrations of Cu was also recorded for nZVI extracted from both unbuffered and pH buffered AMD, however, in contrast to the nZVI extracted from the unbuffered AMD very low (or zero) concentrations of both Al and Zn were detected. Cu concentration maxima of 6.60 at.% was recorded for pH buffered system and attributed to the greater dissolution of Fe (from the nZVI) in such systems which in turn decreased the ratio of solid Fe to Cu.

3.5.3. HRTEM-EDS data

HRTEM-EDS images of the nZVI after exposure to the AMD at a concentration of 1.0 g/L for 4 and 24 h are displayed in Fig. 8 with additional EDS maps displayed in Figures S6 and S7 and metal concentration data displayed in Table 4. It can be observed that Fe, O, Al, Cu, Zn, Si and S comprise >99% of all samples analysed with trace quantities of Mg, Ca, Mn and Cl recorded. Three types of nanomaterial can be observed: (i) "spherical" nanoparticles which exhibit a core-shell structure; (ii) "spherical" nanoparticles which do not exhibit a core-shell structure; and (iii) "needle" or "rod" shaped nanoparticles. The latter two nanomaterials were more prevalent in the samples extracted during the latter periods of the experiment (e.g. >7 d), indicating that they were likely to be either nZVI corrosion products or precipitated native iron (hydr)oxides. In the vast majority of instances Cu was detected as being relatively diffuse (i.e. no clearly defined pure Cu nanoparticles were detected without also being co-located with Fe) for the nanoparticles produced by the exposure of the nZVI to the unbuffered AMD water. In contrast clearly defined discrete Cu-bearing nanoparticles were recorded for the pH buffered system (Figs. 9 and 10). A summary of the physico-chemical properties of such Cu-bearing nanoparticles is displayed in Table 5.

Similar to the nZVI which were exposed to the unbuffered AMD Fe and O were recorded as comprising a major component (i.e. typically >80 wt.%) of the material detected using EDS for the nZVI exposed to pH buffered AMD. However, in contrast no Al or Zn was detected and Cu was detected in higher concentrations. It addition it is observed that a major proportion of the Cu-bearing nanoparticles detected were located in regions that are distinctly separate to the Fe bearing nanoparticles, indicating that they are discrete nanoparticles and thus able to be separated from each other. In some instances, however, the Cu-bearing nanoparticles were recorded as surrounding a larger Fe bearing nanoparticle. This indicates that such Cu nanoparticles are likely formed via a surface mediated process (e.g. the Cu was deposited as a nanoparticulate layer upon the surface of each dissolving nZVI particle).

4. Industrial/environmental implications

Almost all conventional methods for AMD treatment (e.g. alkali dosing or passive bioreactors) are not designed with metal recovery in mind. As such the wastes produced (e.g. ochreous sludges or metal sulphide-rich organics) can require expensive long-term management associated with their treatment and/or disposal. Instead a paradigm shift is required in order to reconsider AMD as a resource rather than simply an environmental liability. One option is to develop novel methods that selectively recover key metals/metalloids from AMD and thus provide economic value in order to offset the costs of such remediation activities. An intrinsic barrier associated with this, however, is that valuable metals in AMD are often present at relatively low concentrations (e.g. <100 mg/L) and as such their recovery and conversion to bulk/sheet metal is not typically economically viable. Instead, if metals could be directly converted into valuable (nano)material products then a clear economic driver could be realised. For example, the current raw metal value of Cu is approximately 6800 USD/t [38] compared to either approximately 10,000 USD/t for bulk orders of Cu° nanoparticles of relatively low purity and unconstrained particle size distributions (PSD) [39] to upwards of approximately >50,000 USD/t for

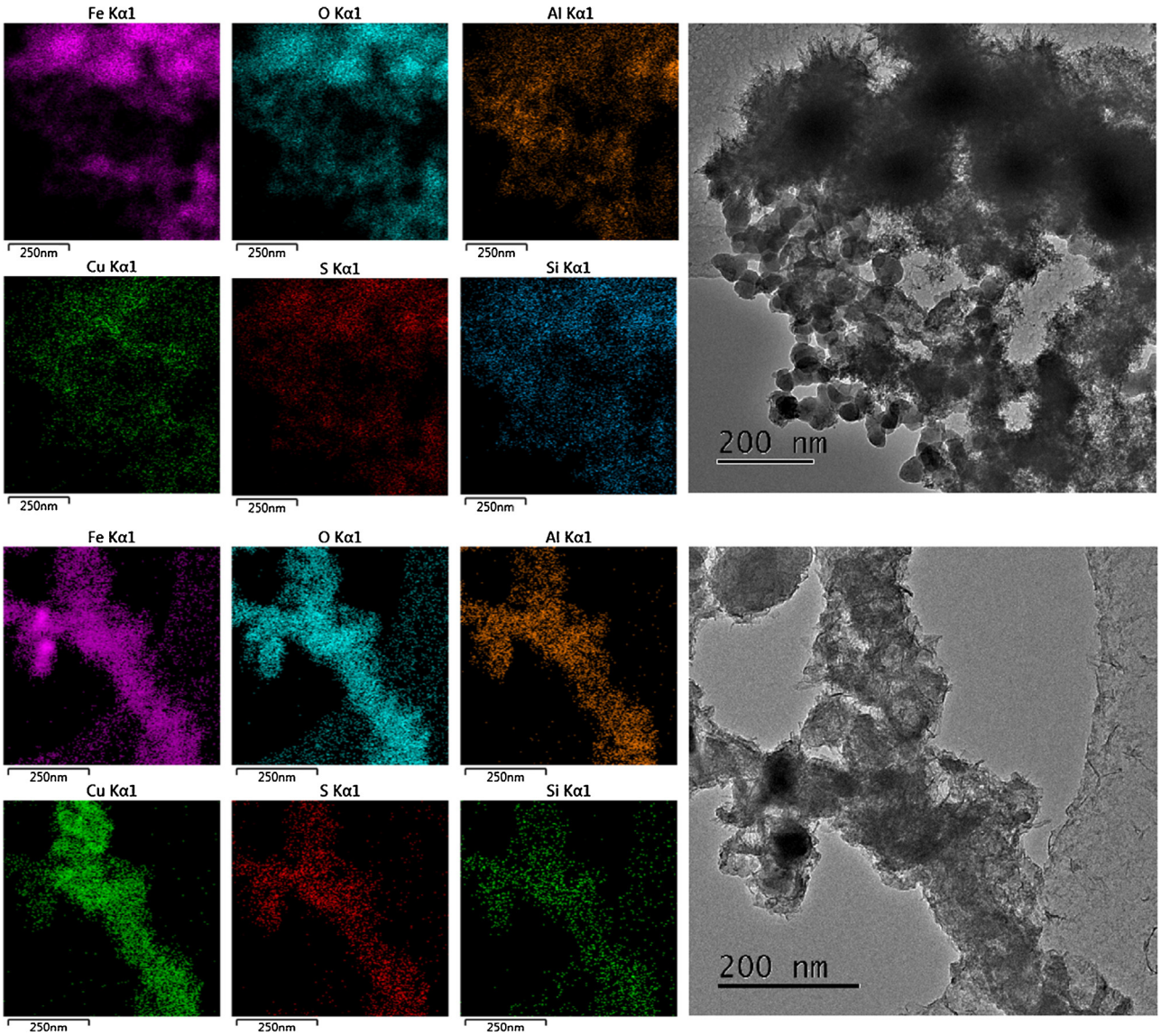

Fig. 8. HRTEM and corresponding EDS maps of the six most abundant elements (by wt.%) of the nZVI after 4 h (top) and 24 h (bottom) exposure to the AMD (no pH buffer). Additional HRTEM images and EDS maps are displayed in Figures S6 and S7. A nZVI concentration of 1.0 g/L was used.

Table 4
Composition (by wt.%) of the nZVI after exposure to the AMD (no pH buffer) after 4, 24, 48 and 168 h as determined using HRTEM-EDS. A nZVI concentration of 1.0 g/L was used.

Element	nZVI composition (wt. %) after 4 hrs exposure to the AMD	nZVI composition (wt. %) after 24 hrs exposure to the AMD	nZVI composition (wt. %) after 48 hrs exposure to the AMD	nZVI composition (wt. %) after 168 hrs exposure to the AMD
O	49.2	47.6	57.2	51.5
Mg	0.2	0.3	0.2	0.1
Al	7.7	5.1	10.4	5.2
Si	1.8	2.8	5.0	3.9
S	2.5	3.3	3.5	4.5
Cl	0.3	0.0	0.0	0.0
Ca	0.2	0.3	0.1	0.3
Mn	0.1	0.0	0.0	0.0
Fe	25.1	37.7	19.5	34.1
Cu	12.4	1.7	2.6	0.4
Zn	0.5	1.2	1.5	0.0

nanopowder of well constrained purity and PSD (e.g. [40]). Aside from this clear economic incentive the formation of nanomaterials directly from waste streams (such as AMD) could also have a significantly positive influence on the economics and sustainability of the nanomaterial production industries.

Here we have demonstrated a new method for the one pot selective formation of Cu bearing nanoparticulate products from AMD

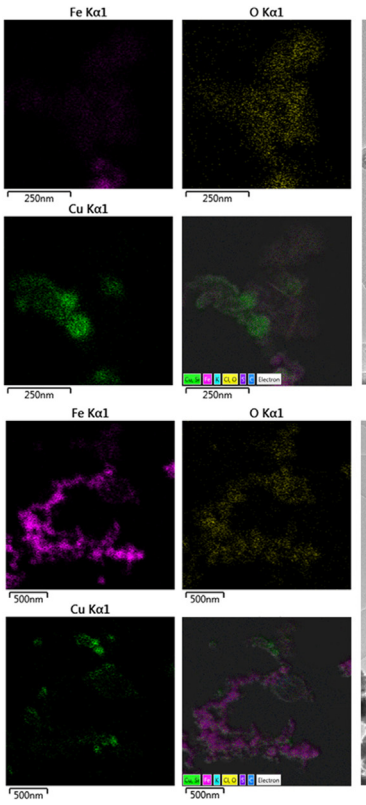

Element	Map (wt. %)	A (wt. %)	B (wt. %)
O	43.0	21.0	19.7
Si	3.2	0.0	1.9
S	0.0	0.0	0.0
Cl	0.0	0.0	0.0
K	1.6	0.0	0.0
Fe	29.3	11.4	14.3
Cu	22.9	67.6	64.1

Element	Map (wt. %)	A (wt. %)	B (wt. %)
O	30.9	34.2	37.4
Si	1.7	0.0	2.4
S	0.5	0.0	0.0
Cl	0.4	0.0	0.0
K	1.5	0.0	0.0
Fe	59.7	36.1	16.2
Cu	5.3	29.7	44.0

Fig. 9. HRTEM-EDS maps along with spectra quantification data for the nZVI (and resultant Cu nanoparticles) following exposure to the pH buffered AMD for 1 h. A nZVI concentration of 1.0 g/L was used. The pH buffer reagents comprised 0.1 g/L $C_8H_5KO_4$ and 0.005M HCl.

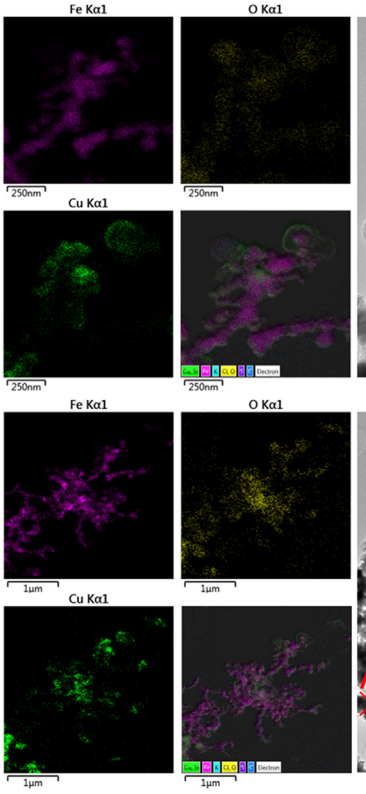

Element	Map (wt. %)	A (wt. %)	B (wt. %)
O	21.4	14.9	27.9
Si	0.6	0.0	0.0
S	0.7	0.0	0.0
Cl	0.0	0.0	0.0
K	0.8	0.0	0.0
Fe	65.1	57.8	24.3
Cu	11.4	27.3	47.8

Element	Map (wt. %)	A (wt. %)	B (wt. %)
O	25.6	26.1	11.3
Si	1.0	0.0	0.0
S	0.7	0.0	0.0
Cl	0.3	0.0	0.0
K	0.9	0.0	0.0
Fe	63.2	41.3	71.1
Cu	8.3	32.6	17.6

Fig. 10. HRTEM-EDS maps along with spectra quantification data for the nZVI (and resultant Cu nanoparticles) following exposure to the pH buffered AMD for 4 h. A nZVI concentration of 1.0 g/L was used. The pH buffer reagents comprised 0.1 g/L $C_8H_5KO_4$ and 0.005M HCl.

Table 5
Physical and chemical properties of the Cu-bearing nanoparticles formed due to the exposure of nZVI to the pH buffered AMD for 1 and 4 h. A nZVI concentration of 1.0 g/L was used. The pH buffer reagents comprised 0.1 g/L $C_8H_5KO_4$ and 0.005M HCl.

Parameter	Analysis technique	1 hour exposure	4 hour exposure
Particle size distribution (%)	HRTEM	0-50nm: 38.1 50-100nm: 47.6 > 100nm: 14.3	0-50nm: 61.5 50-100nm: 30.8 > 100nm: 7.7
Mean particle size (nm)	HRTEM	59.6	47.3
Composition	XPS	Cu°, Cu_2O	Cu°, Cu_2O
Maximum purity detected (wt. % Cu)	HRTEM-EDS	67.6	47.8
Nanoparticle shape	HRTEM	High sphericity, rounded	High sphericity, rounded
Crystallinity	HRTEM	Polycrystalline	Polycrystalline

by simply exposing the AMD to nZVI whilst an acidic pH is maintained. AMD is an ideal candidate waste stream for conversion to nanomaterials because it typically contains appreciable concentrations of high value metals (such as Cu) but is also is a globally significant environmental problem. The Cu nanoparticle synthesis mechanism has been determined to be *via* the cementation of aqueous Cu with nanoscale Fe° which comprises the dissolution of Fe from the nZVI which is coupled to the simultaneous chemical reduction of Cu ions into discrete Cu° nanoparticles. As displayed in Eq. (1) the reaction is spontaneous and results in the conversion of Cu^{2+} to Cu° in a 1:1 M ratio with the oxidation of Fe° to Fe^{2+}. The synthesised nanoscale Cu^0 are then likely to be recoverable using conventional clarification and/or centrifugation processes, which are well proven technologies for nanoparticle recovery (e.g. [41]), with the former typically more cost effective but would require a further step in order to remove the coagulant from the nanomaterial. Whilst being expensive centrifugation could also potentially be utilised, however, for the separation of the Cu nanoparticles from any other unwanted nanoparticles (e.g. nZVI corrosion phases) as a function of their relative density. In addition, the HRTEM data demonstrates that a significant proportion of the Cu nanoparticles are physically bound (electrostatically) to the nZVI, and as such could be recovered using a magnetic field. Other factors to consider includes the requirement for the treatment/recycling of any residual AMD (which will contain elevated aqueous Fe concentrations due to nZVI dissolution) prior to being released back into the environment, however, it is likely that this will be able to be achieved using conventional passive or active AMD treatment processes (e.g. a constructed wetland). Where AMD is anoxic, maintenance of anoxia will also be beneficial for Cu nanoparticle recovery and thereby limit the unwanted reaction between nZVI and DO and thus maximise the proportion of nZVI available for selective Cu nanoparticle formation.

5. Conclusions

Whilst many studies have determined the performance of various different (nano)sorbents for the removal of metals and metalloids from wastewaters/effluents very few have also investigated the physico-chemical composition of the resultant sorbed/precipitated nanomaterial(s). Here nZVI have been investigated for the removal of metals and metalloids from AMD with a particular focus on the synthesis of nanoscale Cu°. The following can be concluded:

AMD treatment required a relatively high concentration of nZVI, with concentrations <0.5 g/L imparting minimal changes to the solution electrochemistry (pH, Eh and DO) and metal/metalloid concentrations.

Addition of nZVI concentrations ≥ 1 g/L to the AMD resulted in the rapid and near total selective removal of Cu, Al and Cd solution (>99.9% removal within 1 h) through a combination of mechanisms including cementation (for Cu), precipitation and sorption to corrosion products (for Al and Cd). In contrast minimal changes in the concentrations of numerous other metal and metalloid ions present in the AMD (namely: Na, Ca, Mg, K, Mn and Zn) were recorded.

Following near total removal of Al, Cu and Cd from the aqueous phase during the initial stages of the reaction (<48 h) significant re-release was recorded and attributed to the reactive exhaustion of the nZVI and ingress of oxygen allowing recovery of system Eh, DO and pH.

The selectivity of nZVI for Cu can be further enhanced by the application of an acidic pH buffer. This is likely due to the restriction of Zn, Cd sorption onto nZVI corrosion products along with the concurrent prevention of hydrolysis and precipitation of Al as $Al(OH)_3$.

The outermost surface of the Cu nanoparticles formed were determined using XPS to comprise a mixture of Cu° and Cu^{2+}, with detection of the former species clear evidence that such nanoparticles formed via a cementation (redox) reaction between aqueous Cu and Fe° from the nZVI.

Overall the results demonstrate that the application of nZVI can be fine-tuned for the highly selective formation of Cu° bearing nanoparticles from acidic wastewater, such as AMD, which might then find application in a wide range of applications including catalysis, optics, electronics and as antifungal/antibacterial agents. The method is easily scalable and does not require any electrical input and is therefore a potentially highly useful "green" method for the upcycling of metals from metal-bearing waters and effluents into high value nanomaterials.

Acknowledgements

We would like to thank Jeff Rowlands and Marco Santonastaso and from the School of Engineering, Cardiff University for their technical support. We would also like to thank Phillip Goodman from Natural Resources Wales for his help organising the mine water sample collection. We would also like to thank Dr Thomas Davies from the Cardiff Catalysis Institute and the Cardiff Electron Microscopy Facility for the HRTEM-EDS analysis and Dr David Morgan from the School of Chemistry, Cardiff University for the XPS and BET surface area analysis. Photographs included in the RHS of the graphic abstract are from the following references (clockwise from top LHS) [42–47]. This work was financially supported by the Natural Environmental Research Council (grant number: NE/L013908/1) and the Camborne School of Mines Trust.

Appendix A. Supplementary data

Supplementary material related to this article can be found, in the online version, at doi:https://doi.org/10.1016/j.jhazmat.2017.12.014.

References

[1] D.B. Johnson, K.B. Hallberg, Acid mine drainage remediation options: a review, Science the Total. Environ. 338 (2005) 3–14.
[2] R.A. Crane, D.E. Sinnett, P.J. Cleall, D.J. Sapsford, Physicochemical composition of wastes and co-located environmental designations at legacy mine sites in the south west of England and Wales: implications for their resource potential, Resour. Conserv. Recycl. 123 (2017) 117–134.
[3] W.M. Mayes, D. Johnston, H.A.B. Potter, A.P. Jarvis, A national strategy for identification, prioritisation and management of pollution from abandoned

non-coal mine sites in England and Wales. I. Methodology development and initial results, Sci. Total Environ. 407 (2009) 5435–5447.
[4] R.L.P. Kleinmann, Acid mine drainage in the united states controlling the impact on streams and rivers University of Toronto, 4th World Congress on the Conservation of the Built and Natural Environments (1989) 1–10.
[5] R.A. Crane, T.B. Scott, The removal of uranium onto nanoscale zero-valent iron in anoxic batch systems, J. Nanomater. 2014 (2014) 1–9.
[6] I.C. Popescu, P. Filip, D. Humelnicu, I. Humelnicu, T.B. Scott, R.A. Crane, Removal of uranium (VI) from aqueous systems by nanoscale zero-valent iron particles suspended in carboxy-methyl cellulose, J. Nucl. Mater. 443 (2013) 250–255.
[7] R.A. Crane, T.B. Scott, Nanoscale zero-valent iron: future prospects for an emerging water treatment technology, J. Haz. Mater. 211 (2012) 112–125.
[8] T.B. Scott, M. Dickinson, R.A. Crane, O. Riba, G. Hughes, G.C. Allen, The effects of vacuum annealing on the structure and surface chemistry of iron nanoparticles, J. Nano Res. 12 (2010) 2081–2092.
[9] C. Noubactep, S. Caré, R.A. Crane, Nanoscale metallic iron for environmental remediation: prospects and limitations, Water Air Soil. Pollut. 223 (2012) 1363–1382.
[10] T.B. Scott, I.C. Popescu, R.A. Crane, C. Noubactep, Nano-scale metallic iron for the treatment of solutions containing multiple inorganic contaminants, J. Hazard. Mater. 186 (2010) 280–287.
[11] R.A. Crane, H. Pullin, J. Macfarlane, M. Silion, I.C. Popescu, M. Andersen, V. Calen, T.B. Scott, Field application of iron and iron-nickel nanoparticles for the ex situ remediation of a uranium bearing mine water effluent, J. Environ. Eng. 141 (2015) 241–259.
[12] R.A. Crane, H. Pullin, T.B. Scott, The influence of calcium, sodium and bicarbonate on the uptake of uranium onto nanoscale zero-valent iron particles, Chem. Eng. J. 277 (2015) 252–259.
[13] R.A. Crane, T.B. Scott, The removal of uranium onto carbon-supported nanoscale zero-valent iron particles, J. Nano Res. 16 (2014) 1–13.
[14] H. Pullin, R.A. Crane, D.J. Morgan, T.B. Scott, The effect of common groundwater anions on the aqueous corrosion of zero-valent iron nanoparticles and associated removal of aqueous copper and zinc, J. Environ. Chem. Eng. 5 (2017) 1166–1173.
[15] S. Li, W. Wang, F. Liang, W.-x Zhang, Heavy metal removal using nanoscale zero-valent iron (nZVI): theory and application, J. Hazard. Mater. 322 (2017) 163–171.
[16] S. Klimkova, M. Cernik, L. Lacinova, J. Filip, D. Jancik, R. Zboril, Zero-valent iron nanoparticles in treatment of acid Mine water from in situ uranium leaching, Chemosphere 82 (2010) 1178–1184.
[17] S.R. Kanel, B. Manning, L. Charlet, H. Choi, Removal of arsenic(III) from groundwater by nanoscale zero-valent iron, Environ. Sci. Technol. 39 (2005) 1291–1298.
[18] S. Choe, Y.Y. Chang, K.Y. Hwang, J. Khim, Kinetics of reductive denitrification by nanoscale zero-valent iron, Chemosphere 41 (2000) 1307–1311.
[19] F. Fagerlund, T.H. Illangasekare, T. Phenrat, H.J. Kim, G.V. Lowry, PCE dissolution and simultaneous dechlorination by nanoscale zero-valent iron in a DNAPL source zone, J. Contam. Hydrol. 131 (2012) 9–28.
[20] T. Phenrat, I. Kumloet, Electromagnetic induction of nanoscale zerovalent iron particles accelerates the degradation of chlorinated dense non-aqueous phase liquid: proof of concept, Water Res. 107 (2016) 19–28.
[21] C.B. Wang, W.X. Zhang, Synthesizing nanoscale iron particles for rapid and complete dechlorination of TCE and pcbs, Environ. Sci. Technol. 31 (1997) 2154–2156.
[22] X. Wei, R.C. Viadero, Synthesis of magnetite nanoparticles with ferric iron recovered from acid mine drainage: implications for environmental engineering, Colloids Surf. A: Physicochem. Eng. Asp. 294 (2007) 280–286.
[23] D. Prabu, R. Parthiban, P.S. Kumar, N. Kumari, P. Saikia, Adsorption of copper ions onto nano-scale zero-valent iron impregnated cashew nut shell, Desalin. Water Treat. 57 (2016) 14.
[24] M.A. Liendo, G.E. Navarro, C.H. Sampaio, Nano and micro ZVI in aqueous media: copper uptake and solution behavior, Water Air Soil Pollut. 224 (2013) 1541.
[25] European Environment, Bureau, The environmental performance of the mining industry and the action necessary to strengthen European legislation in the wake of the tisza-danube pollution, in: EEB Document No 2000/016, 2000, 32pp.
[26] C.M. Kay, O.F. Rowe, L. Rocchetti, K. Coupland, K.B. Hallberg, D.B. Johnson, Evolution of microbial "streamer" growths in an acidic, metal-contaminated stream draining an abandoned underground copper mine, Life 3 (2013) 189–210.
[27] G.N. Glavee, K.J. Klabunde, C.M. Sorensen, G.C. Hadjipanayis, Chemistry of borohydride reduction of iron(II) and iron(III) ions in aqueous and nonaqueous media, formation of nanoscale fe, FeB and Fe2b powders, Inorg. Chem. 34 (1995) 28–35.
[28] C.B. Wang, W.-X. Zhang, Synthesizing nanoscale iron particles for rapid and complete dechlorination of TCE and pcbs, Environ. Sci. Technol. 31 (1997) 2154–2156.
[29] T.B. Scott, G.C. Allen, P.J. Heard, M.G. Randell, Reduction of U(VI) to U(IV) on the surface of magnetite, Geochim. Et Cosmochim. Acta 69 (2005) 5639–5646.
[30] M. Baalousha, Aggregation and disaggregation of iron oxide nanoparticles: influence of particle concentration, pH and natural organic matter, Sci. Tot. Environ. 407 (2009) 2093–2101.
[31] WHO, Guidelines for Drinking-Water Quality, forth edition, 2011, ISBN 9789241548151 http://www.who.int/water_sanitation_health/publications/2011/dwq_guidelines/en/.
[32] R.T. Wilkin, M.S. McNeil, Laboratory evaluation of zero-valent iron to treat water impacted by acid mine drainage, Chemosphere 53 (2003) 715–725.
[33] R.A. Crane, M. Dickinson, I.C. Popescu, T.B. Scott, Magnetite and zero-valent iron nanoparticles for the remediation of uranium contaminated environmental water, Water Res. 45 (2011) 2931–2942.
[34] U. Schwertman, W.R. Fischer, Natural "amorphous" ferric hydroxide, Geoderma 10 (1973) 237–247.
[35] http://www.xpsfitting.com/2008/09/aluminum.html (Accessed 28/02/17).
[36] http://xpssimplified.com/elements/copper.php. (Accessed 28/02/17).
[37] J. Topfer, A. Feltz, D. Graf, B. Hackl, L. Raupach, P. Cation, Valencies and distribution in the spinels NiMn2O4 and MzNiMn2−zO4 (M = li, cu) studied by XPS. weissbrodt, Phys. Status Solidi A 134 (1992) 405.
[38] http://www.infomine.com/investment/metal-prices/copper/ (Accessed 12/09/17).
[39] www.alibaba.com (Accessed 12/09/17) "copper nanopowder" search function.
[40] Copper nanopowder, <100 nm (BET), <3% oxygen passivation, 99% trace metals basis. Product number: 794317-100G; PubChem Substance ID: 329768439; CAS Number: 7440-50-8. URL: www.sigmaaldrich.com (Accessed 12/09/17).
[41] Q. Sun, Y. Li, T. Tang, Z. Yuan, C.-P. Yu, Removal of silver nanoparticles by coagulation processes, J. Hazard. Mater. 261 (2013) 414–420.
[42] https://www.constructioncanada.net/coppers-antimicrobial-properties/ (Accessed 26/05/17).
[43] http://www.happypreppers.com/ducttape.html (Accessed 26/05/17).
[44] http://www.goodwaychemicals.com/lube-additive-packages.html (Accessed 26/05/17).
[45] http://people.duke.edu/~zh28/ (Accessed 26/05/17).
[46] http://www.boltonmetals.com/products/ (Accessed 26/05/17).
[47] https://www.whiteclouds.com/3dpedia-index/conductive-ink (Accessed 26/05/17).